

Journal Pre-proof

Seismic performance evaluation of reactor containment building considering effects of concrete material models and prestressing forces

Bidhek Thusa, Duy-Duan Nguyen, Md Samdani Azad, Tae-Hyung Lee



PII: S1738-5733(23)00075-X

DOI: <https://doi.org/10.1016/j.net.2023.02.004>

Reference: NET 2272

To appear in: *Nuclear Engineering and Technology*

Received Date: 19 October 2022

Revised Date: 23 January 2023

Accepted Date: 3 February 2023

Please cite this article as: B. Thusa, D.-D. Nguyen, M.S. Azad, T.-H. Lee, Seismic performance evaluation of reactor containment building considering effects of concrete material models and prestressing forces, *Nuclear Engineering and Technology* (2023), doi: <https://doi.org/10.1016/j.net.2023.02.004>.

This is a PDF file of an article that has undergone enhancements after acceptance, such as the addition of a cover page and metadata, and formatting for readability, but it is not yet the definitive version of record. This version will undergo additional copyediting, typesetting and review before it is published in its final form, but we are providing this version to give early visibility of the article. Please note that, during the production process, errors may be discovered which could affect the content, and all legal disclaimers that apply to the journal pertain.

© 2023 Korean Nuclear Society, Published by Elsevier Korea LLC. All rights reserved.

Seismic performance evaluation of reactor containment building considering effects of concrete material models and prestressing forces

Bidhek Thusa¹, Duy-Duan Nguyen², Md. Samdani Azad¹, Tae-Hyung Lee^{1,*}

¹*Department of Civil and Environmental Engineering, Konkuk University, Seoul 05029, Korea*

²*Department of Civil Engineering, Vinh University, Vinh 461010, Vietnam*

**Corresponding author, email: thlee@konkuk.ac.kr*

Abstract

The reactor containment building (RCB) in nuclear power plants (NPPs) plays an important role in protecting the reactor systems from external loads as well as preventing radioactive leaking. As we witnessed the nuclear disaster at Fukushima Daiichi (Japan) in 2011, the earthquake is one of the major threats to NPPs. The purpose of this study is to evaluate effects of concrete material models and prestressing forces on the seismic performance evaluation of RCB in NPPs. A typical RCB designed in Korea is employed for a case study. Detailed three-dimensional nonlinear finite element models of RCB are developed in ANSYS. A series of pushover analyses are then performed to obtain the pushover curves of RCB. Different capacity curves are compared to recognize the influence of different material models on the nonlinear behavior of RCB. Additionally, the effects of prestressing forces on the seismic performances of the structure are also investigated. Moreover, a set of damage states corresponding to damage evolutions of the structures is proposed in this study.

Keywords: nuclear power plant; three-dimensional finite element model; pushover analysis; concrete model; prestressing force

1. Introduction

The number of nuclear power plants (NPPs) has been growing around the world and playing as the second major energy source for decades. However, the Chernobyl (Ukraine, 1986) and Fukushima Daiichi (Japan, 2011) nuclear disasters have taught us well about the serious impact of the nuclear disaster on the natural environment, human beings, and economic values. The radioactive leakage from a nuclear containment

29 structure can cause catastrophic consequences. Thus, the reactor containment building (RCB) is considered
30 the most important structure in nuclear power plants.

31 The seismic performance of NPP structures is commonly evaluated using probabilistic approaches [1-9],
32 in which the influences of input structural variables or earthquakes need to be investigated sufficiently. Effects
33 of uncertainty in different modeling parameters to RCBs were addressed in previous studies [10-15]. Also,
34 many studies studied the effects of earthquake characteristics on the performance of NPP structures such as
35 mainshock-aftershock [16, 17], near-fault motions [18-20], far-fault motions [21, 22], site-specific ground
36 motions [23, 24], duration of motions [25], and frequency content [26, 27]. Recently, Nguyen et al. [28] studied
37 the efficiency of various structural modeling schemes on evaluating seismic performance and fragility of an
38 RCB. They emphasized that the linear analysis might underestimate the probability of damage of RCB at a
39 given earthquake intensity when compared to the nonlinear analysis.

40 However, effects of prestressing forces are not properly considered in most of the numerical analysis of
41 such studies. Even though a limited number of studies considered the presence of prestressing forces in their
42 numerical models of various RCBs [29-40], they mostly focused on the performance of RCBs against the
43 internal loads or pressures, not seismic effects.

44 To improve the structural capacity of NPP structures, the use of high-strength concrete materials is a
45 promising solution. Choun and Park [41, 42] investigated the influences of fiber reinforced concrete on the
46 pressure capacity of a prestressed concrete containment vessel (PCCV) structure. They considered two types
47 of fibers, i.e. steel and polyamide. They concluded that the pressure capacity of PCCV with 1% volume of
48 steel fibers was increased by 12% in comparison to a conventional PCCV, while 1.5% volume of polyamide
49 fibers increased the pressure capacity of PCCV by 3%. However, the aforesaid study mainly focused on the
50 ultimate pressure capacity and the failure mechanism under the internal pressure. The seismic response
51 analyses of RCB considering different concrete materials were not systematically conducted yet.

52 The purpose of this study is to evaluate the effects of various concrete material models and prestressing
53 forces on the nonlinear seismic behavior of RCB. Four different concrete models are considered in this study,
54 namely, high-performance concrete (HPC), steel fiber reinforced concrete (SFRC), polyamide fiber reinforced
55 concrete (PFRC), and normal concrete with a compressive strength of 40 MPa (M40). For numerical analyses,

56 three-dimensional finite element models (3D FEM) are developed in ANSYS, a commercial software. To
 57 evaluate the capacity of RCB, pushover analyses are performed with different material models and
 58 with/without prestressing forces. Furthermore, a set of damages states of the non-prestressed and prestressed
 59 RCB structures are proposed, which can be useful for a fragility analysis of such structure.

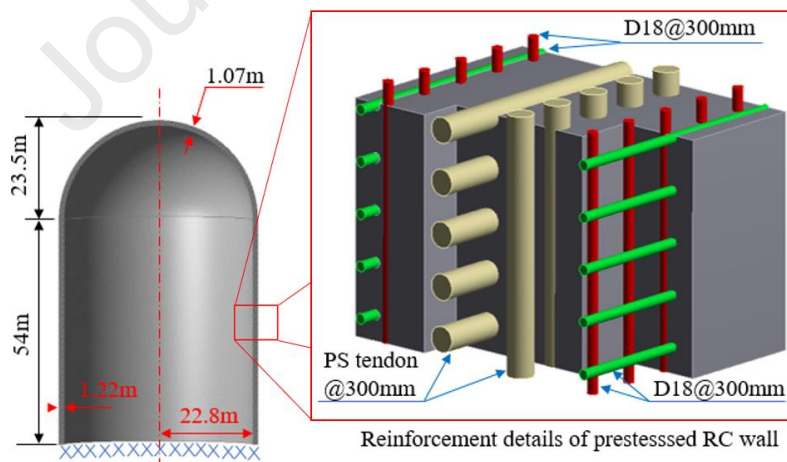
60

61 2. Modeling of RCB

62 2.1. Structural configuration

63 RCB of one of the Korean NPPs is selected for numerical analyses. The reactor containment cylinder has 22.8
 64 m inner radius, 54 m height, and 1.22 m thickness. The inner radius of the dome is 22.8 m, the average thickness
 65 is 1.07 m making the final height of dome as 23.5m. Structural dimensions and reinforcement details of the
 66 structure are shown in Fig. 1. There are two layers of reinforcement with both layers consisting of vertical and
 67 horizontal bars of 18 mm diameter with the spacing of 300 mm. In addition, the RCB wall is prestressed with
 68 post-tensioning tendons. The tendons are anchored between alternate buttresses at 180 degrees. All tendons
 69 are tensioned from both ends. The details of the prestressing tendons are also shown in Fig. 1. It consists of
 70 two layers of the post-tensioning tendons along with the horizontal and vertical directions.

71



72

73

74

75

76

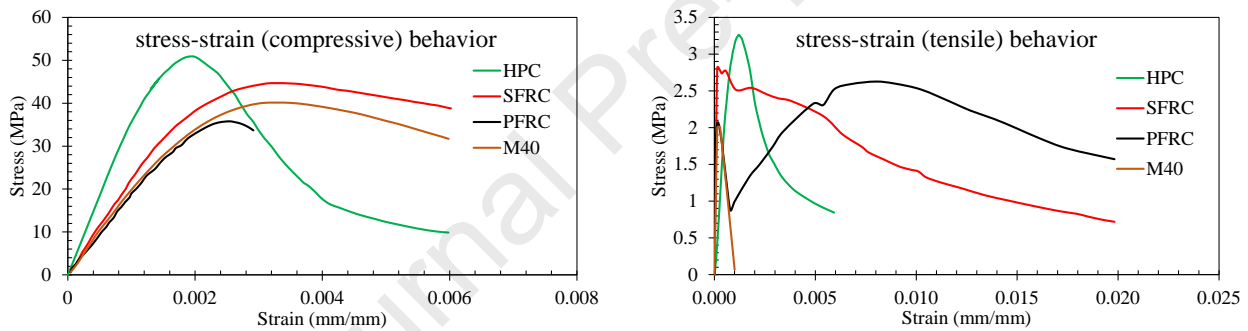
Fig. 1. Dimensions and reinforcement details of RCB

77 2.2. Material properties

78 2.2.1. Nonlinear concrete material models

79 ANSYS [43] provides a large number of material models in its material library. For this study, four isotropic
 80 nonlinear concrete material models are used to investigate the effects of different concrete material models on
 81 the seismic behavior of RCB. Fig. 2 presents the nonlinear stress-strain relationships of various concrete
 82 material models used in this study. The material models considered in this study are high-performance concrete
 83 (HPC), steel fiber reinforced concrete (SFRC), polyamide fiber reinforced concrete (PFRC), and plain concrete
 84 with a compressive strength of 40 MPa (referred to as M40). It should be noted that, in addition to a difference
 85 in the compressive stress, the tensile stresses and corresponding strains of investigated materials are
 86 significantly different. The mechanical properties of concrete models are given in Table 1.

87



88

Fig. 2. Stress-strain relationship of different concrete material models

89

90 For stress-strain curves in the compressive behavior, PFRC has a smaller strain and peak stress
 91 compared to that of other materials. Additionally, HPC, SFRC, and M40 show a similar strain capacity in
 92 compression. Meanwhile, it is observed that there is a large difference in stress-strain curves for tensile
 93 behavior. M40 demonstrates the smallest tensile strain capacity, followed by HPC. SFRC and PFRC exhibit a
 94 very high tensile strain. Specifically, the PFRC material shows a distinct tensile behavior, at first the stress
 95 increases then later it decreases to close to half the peak then again increases. Moreover, it can be found that
 96 PFRC and M40 have a lower tensile stress compared to that of HPC and SFRC models.

97

98

99 Table 1. Mechanical properties of various concrete material models

Material	Compressive strength (MPa)	Tensile strength (MPa)	Elastic modulus (MPa)	Density (kg/m ³)
HPC	51.0	3.26	32,000	2,450
SFRC	44.7	2.80	22,058	2,360
PFRC	35.8	2.62	19,227	1,860
M40	40.2	2.00	20,134	2,350

100

101 **2.2.2. Reinforcing bars and prestressing tendons**

102 Reinforcing bars and prestressing tendons are modeled as bilinear isotropic materials. Both reinforcing bars
 103 and prestressing tendons are modeled according to the overall modeling method with bonded contact with
 104 concrete. Their mechanical properties are given in Table 2.

105

106 Table 2. Mechanical properties of reinforcing bars and prestressing tendons

Material	Yield strength (MPa)	Ultimate strength (MPa)	Elastic modulus (MPa)	Coefficient of thermal expansion (C ⁻¹)
Reinforcing bar				
Steel NL	400	600	200,000	-
Prestressing tendon				
Steel NL	1,670	1,860	195,000	1.2E-5

107

108 **2.3. Application of prestressing forces on tendons**

109 The prestressing force can be applied to a numerical model of a structure through the equivalent strain and
 110 stress or the lowering temperature methods. The lowering temperature method is employed in this study where
 111 the temperature of prestressing tendons are lowered to reflect the interaction force due to the prestressing action.
 112 In this process, the equivalent lowering temperature is calculated for the specific value of the prestressing force
 113 through the thermal contraction of tendons according to the following equation:

$$\Delta T = \frac{P}{E * A * \delta} \quad (1)$$

114 where ΔT is the lowering the temperature; P is the prestressing force; E is the elastic modulus of prestressing
 115 tendons; A is the cross-sectional area of a prestressing tendon; and δ is the coefficient of the thermal expansion
 116 of a prestressing tendon. In this study, the lowering temperature is calculated as -673°C . The temperature can
 117 be calculated by adopting different prestressing levels. In general, a prestressing force is considered to be 60
 118 to 75% of the ultimate tensile strength of prestressing tendons. The prestressing force applied in this study is
 119 70% of the ultimate tensile strength of a prestressing tendon.

120

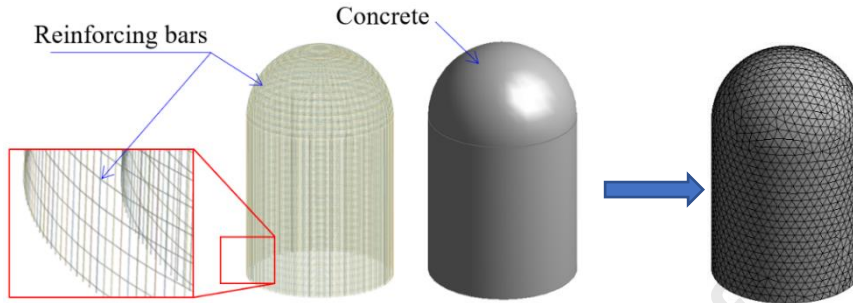
121 **2.4. Numerical model of RCB**

122 A 3D FEM with continuum elements is commonly considered as one of the best modeling approaches of
 123 structures. In particular, 3D FEM with embedded reinforcing bars is a promising modeling technique for
 124 reinforced concrete structures. The cylindrical wall of RCB contains horizontal hoops and vertical reinforcing
 125 bars while the dome contains hoops and radial reinforcements. The numerical models of RCB are developed
 126 within the capability of ANSYS where the modeling process of the reinforced concrete portion and the addition
 127 of prestressing tendons are depicted in Figs. 3 and 4, respectively.

128 To construct 3D FEM without prestressing tendons as shown in Fig. 3, the *solid187* element is used for
 129 concrete, the *beam189* element is used for reinforcing bars, and the *conta175* is utilized to model the contact
 130 element between the concrete and reinforcements. The *solid187* element is a higher order 10-node solid
 131 element with a quadratic displacement behavior. There are three degrees of freedom, i.e., three translations in
 132 X, Y, and Z directions, at each node of this element. The *solid187* element has plasticity, hyper elasticity,
 133 creep, stress stiffening, large deflection, and large strain capabilities. The *Beam189* element is a quadratic 3-
 134 node 3D beam element, which contains six to seven degrees of freedom at each node, i.e., translations in the
 135 X, Y, and Z axes and rotations about these axes. This beam element includes elasticity, plasticity, creep, and
 136 nonlinear material models. Meanwhile, the *conta175* element represents the contact and sliding between a line
 137 and a surface in 2D or 3D. A contact occurs when the element surface penetrates one of the target elements on
 138 a specified target surface. Also, the *conta175* element can be applicable to simulate the delamination at the

139 interface. The model was meshed into 310,122 prism solid elements after conducting a mesh-convergence test.
 140 It is assumed that the base of the structure was fixed to the ground.

141

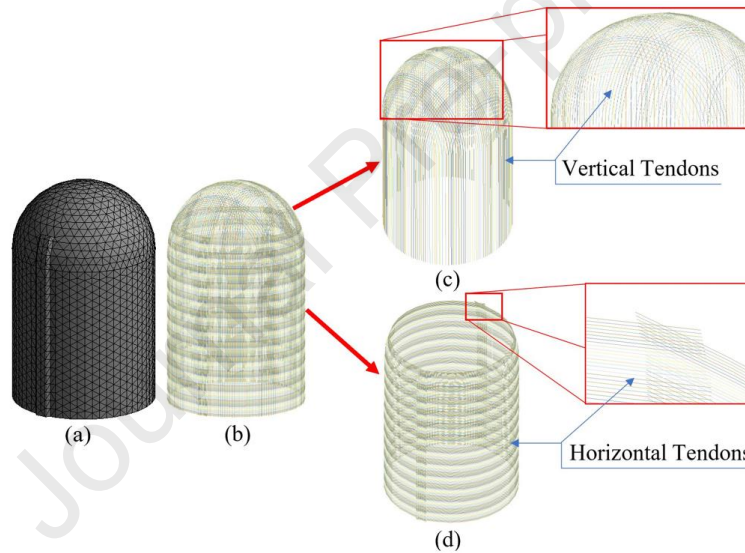


142

143

Fig. 3. A finite element modeling of RCB without prestressing tendons.

144



145

146

Fig. 4. A finite element modeling of RCB with prestressing tendons.

147

148 Finite elements of the prestressing tendons are added to FEM of the reinforced concrete RCB as shown
 149 in Fig. 4. In RCB, prestressing forces are applied separately for horizontal and vertical tendons. For horizontal
 150 tendons, each strand covers half of the cylindrical wall, so each tendon was anchored on the alternate buttress
 151 at 180 degrees' arrangement. These horizontal tendons are placed at 300 mm spacing, as shown in Fig. 4(d).
 152 Accordingly, a total of 165 and 30 tendons are arranged in the cylindrical wall and on the dome of RCB,
 153 respectively [44]. Meanwhile, 100 U-shaped vertical tendons are arranged in the spacing of 750 mm. Each
 154 tendon line with a cross-sectional area of $5,825 \text{ mm}^2$ consists of 42 seven-wire strands with a nominal diameter

155 of 15.2 mm. The tendon's arrangement details are also shown in Fig. 4. The prestressing tendons are modeled
 156 as bonded beam elements to the concrete. The *beam189* element is used to model prestressing tendons.

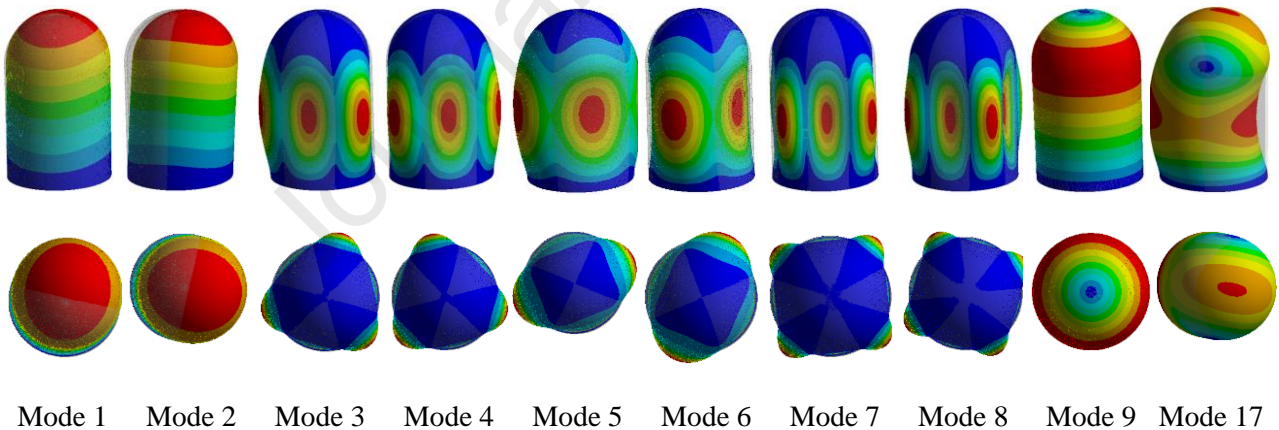
157

158 2.5. Eigenvalue analyses

159 Eigenvalue analyses for the FE models with and without prestressing tendons are performed to compare
 160 vibrational mode shapes and the corresponding frequencies. Figs. 5 and 6 show the selected mode shapes of
 161 the FE model without prestressing tendons and the one with prestressing tendons, respectively. It is observed
 162 that the 3rd and 4th modes of one model and the 5th and 6th modes of the other model are comparable. The
 163 first torsional mode of the model without a prestressing tendon is the 9th and it is comparable to the 7th mode
 164 of the model with prestressing tendons. The corresponding natural frequencies of the vibrational modes
 165 presented in Fig. 5 and Fig. 6 are listed in Table 3. The numerical model with prestressing tendons is
 166 approximately 3% stiffer than that without a prestressing tendon.

167

168



169

Fig. 5. Vibration mode shapes of the FEM without prestressing tendons

170

171

172

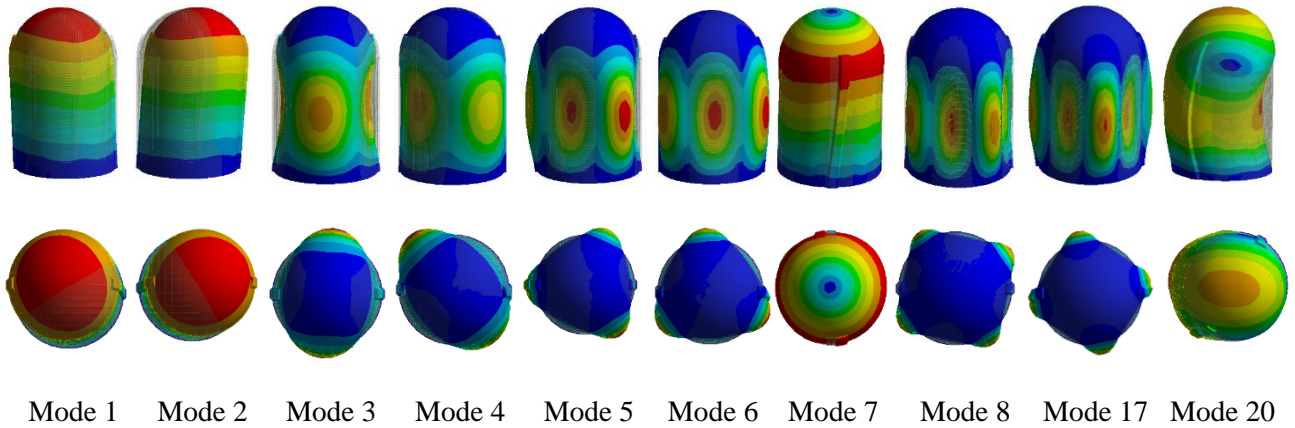


Fig. 6. Vibration mode shapes of the FEM with prestressing tendons

Table 3. Natural frequencies (Hz) of different numerical models of RCB

Mode	Non-presstressed model	Prestressed model
1	4.588	4.719
2	4.635	4.770
3	8.274	8.252
4	8.359	8.419
5	8.558	8.639
6	8.615	8.755
7	9.775	9.853
8	11.189	11.557
9 (17)	11.327	11.664
17 (20)	13.69	13.944

3. Seismic capacity evaluation of RCB

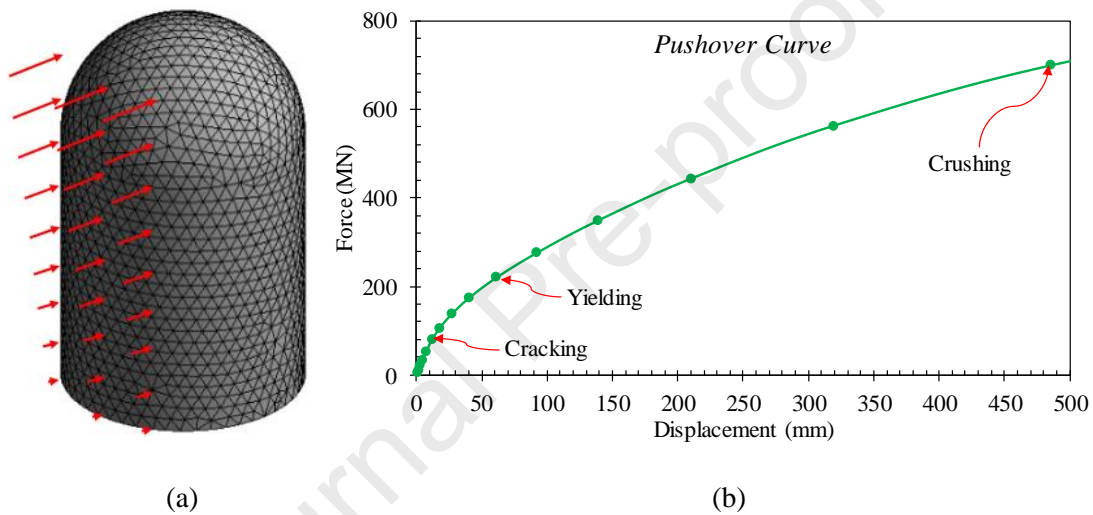
3.1. Pushover analyses

The base shear-deformation curve of a structure is commonly known as a capacity curve which can be obtained from a pushover analysis. Through the capacity curve, different cumulative damages of the structure can be identified. There are proposed definitions of damage states for shear walls in buildings [43] and nuclear facilities [44]. However, since RCB is a special structure combining a dome and a cylinder, it is different from other conventional RC wall structures. A specific guideline for defining damage states of such structure is not proposed yet. Therefore, damage states should be defined based on the capacity of the structure itself rather than adopting existing references, which were proposed for common plane shear walls. In this study, a

186 pushover analysis is performed to obtain the capacity curve and identify the cumulative damages of the
 187 structure.

188 The top lateral displacement is a critical response of RCB since it is a simple cantilever-type structure
 189 [17, 18, 45]. Pushover analyses are performed to determine the force-displacement relationships and the
 190 performance levels of the structural models. The applied load has an inverted-triangular shape as shown in Fig.
 191 7(a). Fig. 7(b) presents the load-displacement relationship where the initiations of cracking, yielding, and
 192 crushing are indicated.

193



194

195

196

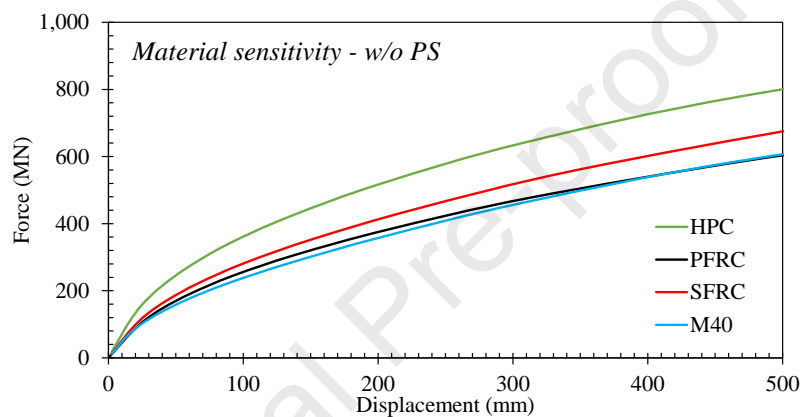
Fig. 7. Pushover analysis of RCB; (a) load distribution and (b) capacity curve.

197

198 3.2. Effect of various concrete material models

199 Pushover analyses are performed for each of the numerical models with a specific concrete material model.
 200 Four concrete material models presented in Fig. 2 were employed in numerical modelings of RCB with or
 201 without prestressing forces. Fig. 8 shows the base shear-displacement relationships of RCB with various
 202 concrete material models without prestressing forces. It is observed that the material models affect the capacity
 203 curves of RCB significantly. The nonlinear behavior starts at the top displacement of 10 mm for all concrete
 204 materials except for HPC, while for HPC, the nonlinear behavior starts at the top displacement of 15 mm. The
 205 structural capacity of RCB with the HPC model is the highest among the studied group and is followed by
 206 RCB with SFRC, PFRC, and M40 models. The strengths of RCB with HPC and SFRC models are 32.5% and

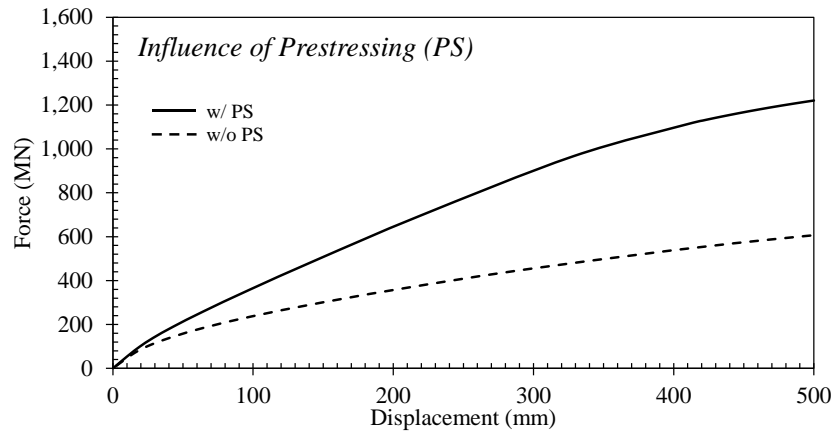
207 11.8% higher than that of the M40 model, respectively. RCB with the PFRC model does not improve the
 208 structural capacity in comparison with that using the M40 model. This is attributed to the reason that the used
 209 PFRC material contains a lower value of elastic modulus and compressive strength in comparison to all the
 210 other material models, as shown in Table 1. However, if we observe the performance of PFRC with a view
 211 that it is the weakest material model presented in this study, it is having almost similar seismic performance
 212 (less than 3% discrepancy) with M40. The distinct S_S curve for tensile behavior of PFRC can be the reason
 213 for PFRC giving comparable performance with M40. These results agree with previous studies [41, 42].
 214



215
 216 Fig. 8. Influence of various concrete material models
 217

218 3.3. Effect of prestressing forces

219 Nonlinear static pushover analyses are performed for RCB models with and without prestressing forces to
 220 study effects of prestressing forces on the seismic capacity of RCB. Fig. 9 shows the capacity curves of RCB
 221 with and without prestressing forces where the M40 model is used for both numerical models. One can observe
 222 the significance of prestressing forces on the seismic capacity of RCB. The capacity curve of RCB with
 223 prestressing forces deviates from that without a prestressing force from around the start of nonlinearity of the
 224 curve. As the displacement increases, the discrepancy becomes larger.
 225



226

227

Fig. 9. Pushover curves of RCB with and without prestressing forces for the M40 concrete model.

228

229

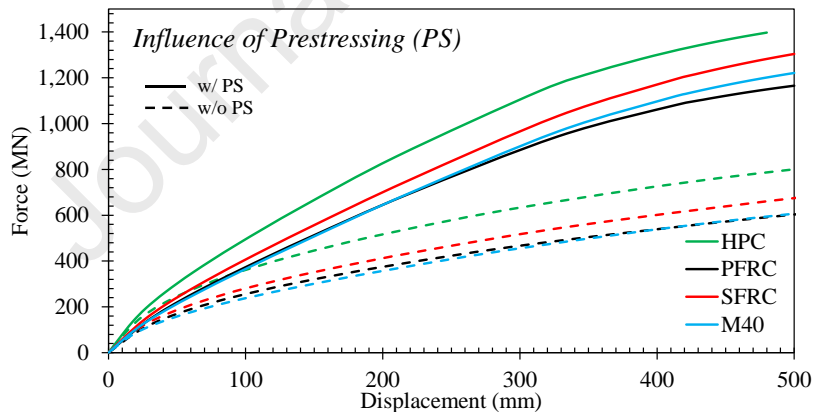
230

231

232

233

Fig. 10 shows the capacity curves of RCB with different material models with and without prestressing forces. It is observed that strengths of RCB with prestressing forces for all concrete material models are 29-30% higher than those of RCB without prestressing forces at the initiation of the yielding. After the yielding, the difference of the strength increases to 43% to 48%.



234

235

Fig. 10. Effects of prestressing forces for various concrete models

236

237

3.4. Proposed damage states

238

239

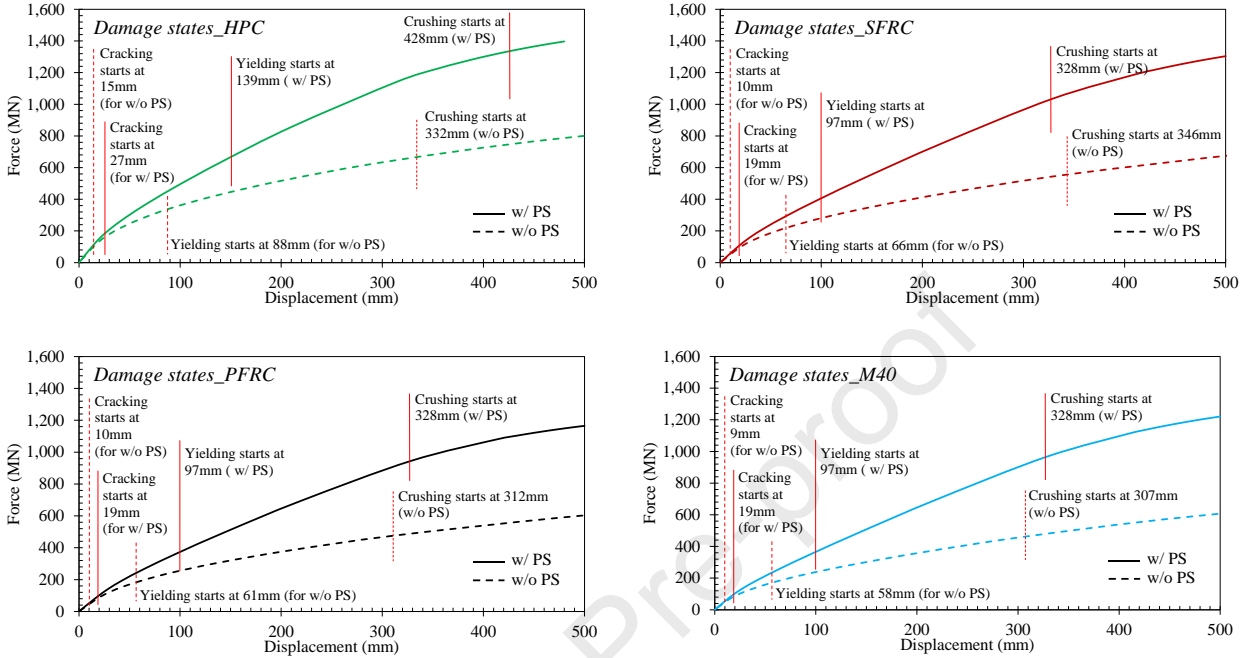
240

241

States of cumulative damage of RCB are monitored during pushover analyses and indicated in Fig. 11. Three proposed damage states are the initiation of the concrete cracking as a minor damage, the initiation of the rebar yielding as a moderate damage, and the initiation of the concrete crushing as an extensive damage. They are referred to as DS1, DS2, and DS3, respectively. This approach is also consistent with studies elsewhere [17,

242 46]. Table 5 presents the proposed damage states and corresponding damage indices for RCB with various
 243 concrete material models.

244



245 Fig. 11. Specified damage states for RCB structure

246

247 For all material models and all damage states, the strength capacity of the prestressed RCB is higher than that
 248 of non-prestressed RCB. The displacement capacity of the prestressed RCB is higher than that of the non-
 249 prestressed RCB for all combinations of material models and damage states, except for the case of SFRC-DS3
 250 where the displacement capacity of the prestressed RCB is slightly lower than that of the non-prestressed RCB.
 251 One can notice that the displacement capacity of the prestressed RCB at DS3 is only slightly higher than that
 252 of the non-prestressed RCB, for cases of PFRC and M40. Introducing a prestressing force to a structure
 253 improves the strength capacity, but it does not necessarily improve the displacement capacity corresponding
 254 to the crushing damage state.

255

256 Table 5. Defined limit states of RCB based on pushover analyses

Concrete Model	Damage state	Base shear (MN)		Displ. (cm)		Drift (%)		Description
		w/o PS	w/ PS	w/o PS	w/ PS	w/o PS	w/ PS	

	DS1 (Minor)	107.38	194.85	1.55	2.75	0.02	0.04	Concrete cracking
HPC	DS2 (Moderate)	339.57	632.77	8.90	13.99	0.11	0.18	Rebar yielding
	DS3 (Extensive)	662.31	1338.78	33.27	42.85	0.43	0.55	Concrete crushing
	DS1 (Minor)	51.27	107.92	1.01	1.91	0.01	0.02	Concrete cracking
SFRC	DS2 (Moderate)	222.47	397.36	6.69	9.72	0.09	0.12	Rebar yielding
	DS3 (Extensive)	558.87	1034.01	34.63	32.83	0.44	0.42	Concrete crushing
	DS1 (Minor)	48.83	96.52	1.08	1.90	0.01	0.2	Concrete cracking
PFRC	DS2 (Moderate)	192.10	365.23	6.13	9.71	0.08	0.12	Rebar yielding
	DS3 (Extensive)	476.77	945.02	31.23	32.82	0.40	0.42	Concrete crushing
	DS1 (Minor)	44.38	98.49	0.94	1.90	0.01	0.02	Concrete cracking
M40	DS2 (Moderate)	174.08	357.40	5.81	9.71	0.07	0.12	Rebar yielding
	DS3 (Extensive)	461.86	966.53	30.71	32.82	0.39	0.42	Concrete crushing

257

258 Fig. 12 presents the base shear at various damage states for different concrete models. RCB with the
259 HPC model shows higher performance to withstand the lateral force due to the seismic load than RCBs with
260 all other concrete material models. Base shears at DS1, DS2, and DS3 for RCB with the HPC model and
261 without prestressing forces is 1.97, 1.77, and 1.38 times those of RCB with the M40 model without a
262 prestressing force, respectively. For RCB with prestressing forces, base shears at DS1, DS2, and DS3 for the
263 HPC model are 2.42, 1.95, and 1.43 times those of the M40 model. On the other hand, RCBs with SFRC,
264 PFRC, and M40 models have comparable damage capacities for all three damage states.

265

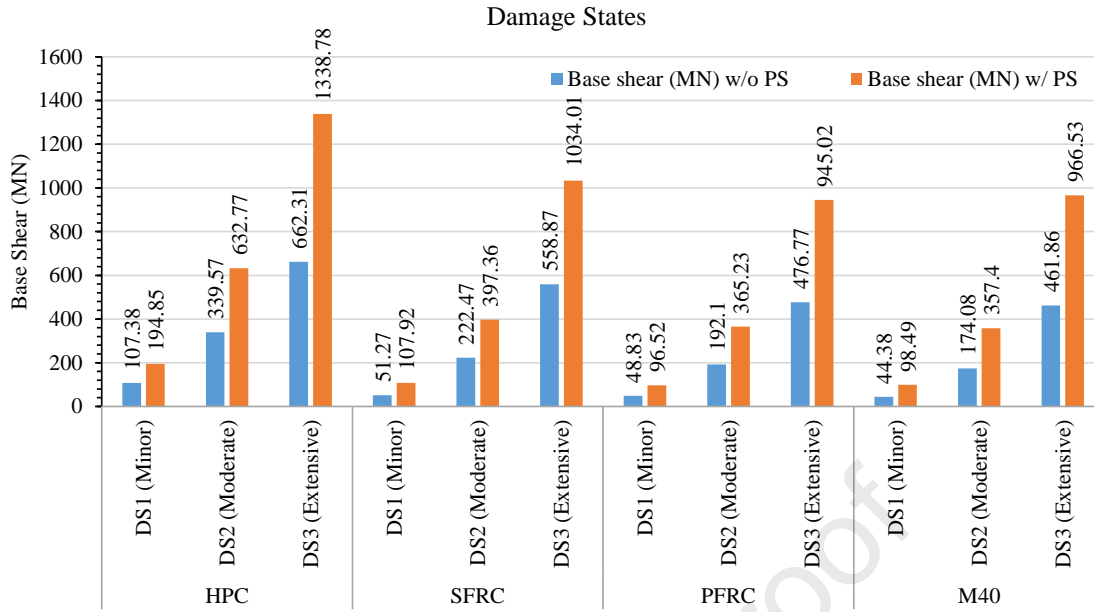


Fig. 12. Base shears at various DSs with respect to various concrete materials

To observe the effect of prestressing forces, the base shear at DS1 for RCB with the HPC model with prestressing forces is 1.82 times that for the same model without a prestressing force. For RCB with the SFRC model, this ratio, i.e. the base shear at DS1 of RCB with prestressing forces to that without a prestressing force, is 2.10, while for PFRC and M40, they are 1.97 and 2.20, respectively.

A similar pattern is observed for all models with and without prestressing forces at DS2 and DS3. At DS2, the aforementioned ratios for the HPC, SFRC, PFRC, and M40 models are 1.86, 1.78, 1.90, and 2.05, respectively. At DS3, the ratios for the HPC, SFRC, PFRC, and M40 models are 2.02, 1.85, 1.98, and 2.09, respectively. Therefore, the base shear capacity of RCB with prestressing forces is around two time that without a prestressing force, for all damage states and for all concrete models. This indicates that the consideration of prestressing forces in a numerical analysis of RCB is crucial for a reliable and accurate assessment of the seismic performance.

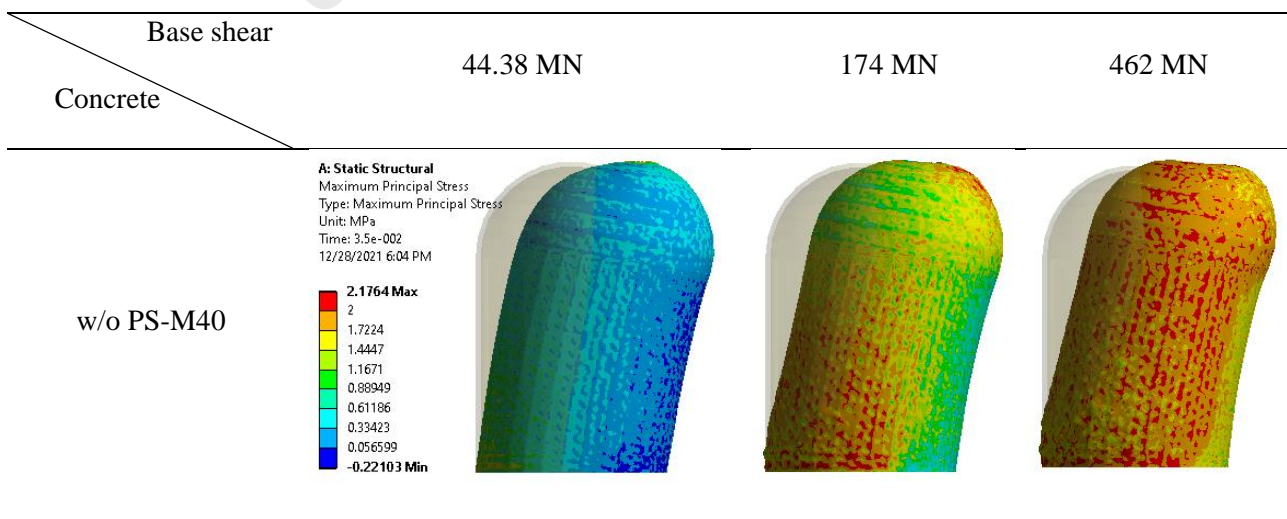
To investigate the effect of material properties and the effect of prestressing forces on local responses of RCB, the maximum principal stresses are monitored. Table 6 shows the maximum principal stress distributions at specific load levels for RCBs with different material models. The base shear capacities of RCB with the M40 model without a prestressing force are taken as the reference load levels, i.e. 44.38 MN, 174

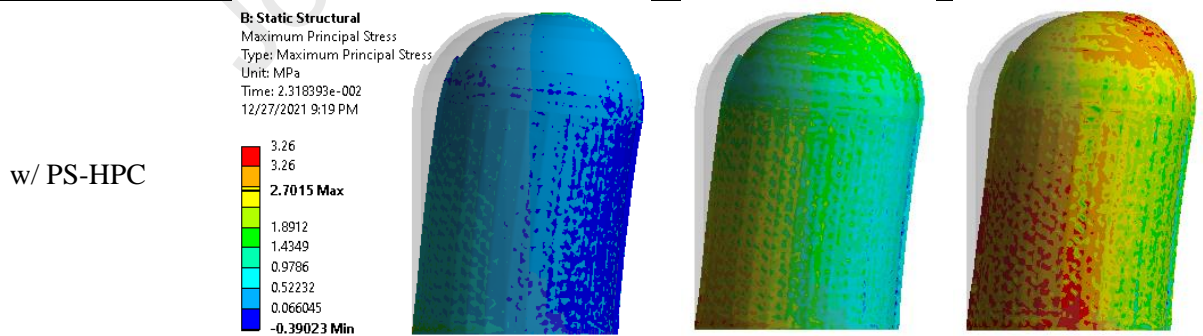
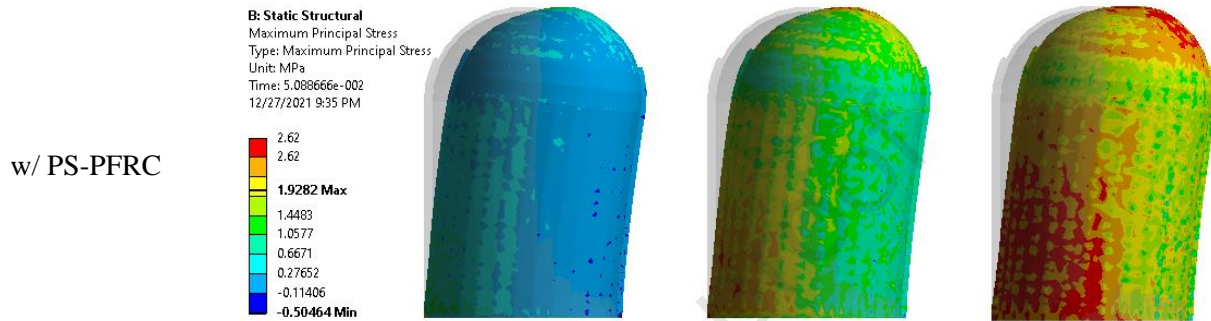
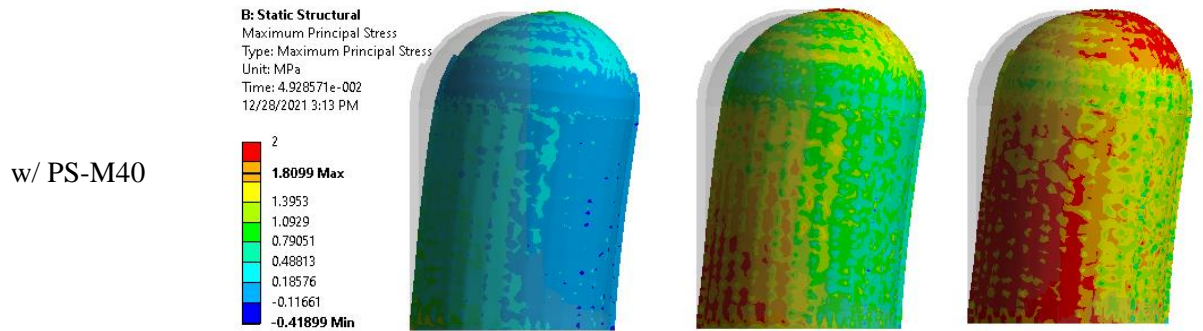
284 MN, and 462 MN for DS1, DS2, and DS3, respectively. The first row of Table 6 shows the maximum principal
 285 stress distribution of RCB with the M40 model without prestressing forces at different damage states. It is
 286 observed that cracks occurs when the tensile stress in concrete reaches 2.0 MPa, then cracks propagate from
 287 just above the support towards the cylindrical part of RCB. At the initiation of the yielding (DS2), cracks are
 288 observed at the dome, too. Finally, at DS3, cracks are extensively spread to RCB.

289 From the second row to the fifth, the maximum principal stress distributions of RCB with the M40, PFRC,
 290 SFRC, and HPC models with prestressing forces are presented, respectively. It should be noted that cracks
 291 occurred if the tensile stress of concrete reached 2.62 MPa, 2.80 MPa, and 3.26 MPa for PFRC, SFRC, and
 292 HPC materials, respectively. The distributions are captured at the reference load levels. The pattern of the
 293 crack propagation is similar for all RCB with different material models. However, the level of the crack
 294 distribution is different for different material models. For a same load level, RCB with the HPC model is the
 295 least damaged. At the 44.38 MN base shear level, no crack is observed from any of the RCB models with
 296 prestressing forces. At the 174 MN base shear level, cracks are observed in a very limited area of RCB with
 297 the M40 model, while no crack is observed in RCB with the other concrete models. These results demonstrate
 298 a significant reduction in concrete cracking and rebar yielding in the HPC model, followed by the SFRC and
 299 PFRC models in comparison to the M40 model.

300

301 Table 6. Evolution of the principal stresses of RCB at different base shears





302

303 **4. Conclusions**

304 This study evaluates the seismic capacity of RCB accounting for the effects of various concrete materials,
 305 namely, PFRC, SFRC, and HPC, and prestressing forces. A nonlinear 3D FEM of RCB is developed using
 306 ANSYS, a commercial software, and a series of pushover analyses are performed. A parametric study is then

307 conducted considering various concrete materials and prestressing forces. The following conclusions are
308 drawn based on numerical analyses.

- 309 • HPC improves the strength capacity of RCB significantly, while SFRC improves it moderately, in
310 comparison to a normal concrete.
- 311 • Prestressing forces improve the seismic capacity of RCB significantly in comparison to that of a non-
312 prestressed RCB as the strength is improved up to 30% at the initiation of yielding, for all concrete
313 material models considered in this study. It convinces us that the consideration of prestressing forces
314 is necessary in a numerical analysis of RCB, which is neglected in many previous studies.
- 315 • The base shear capacity of RCB with prestressing forces at each of the three damage states is around
316 twice that of RCB without prestressing forces for all material models.

317

318 **Conflicts of interest**

319 The authors declare that they have no conflicts of interest.

320

321 **Author's contributions statement**

322 List of Authors: Bidhek Thusa (B.T.), Duy-Duan Nguyen (D.D.N.), Md Samdani Azad (M.S.A.), Tae-Hyung
323 Lee (T.H.L.)

324 Conceptualization: B.T.; Methodology: B.T.; Software and FEM model: B.T.; Formal analysis, B.T.;
325 Investigation, B.T.; Writing—original draft preparation, B.T.; Writing—review and editing of the original
326 draft: B.T. D.D.N.; Writing—review and editing of the first draft: B.T., D.D.N., M.S.A., T.H.L. Writing—
327 review and editing of the final draft: B.T., D.D.N., M.S.A., T.H.L. Project administration: T.H.L.; Supervision:
328 T.H.L.; Funding acquisition, T.H.L. All authors have read and agreed to the published version of the manuscript.

329

330 **Acknowledgment**

331 This research is supported by the Korea Institute of Energy Technology Evaluation and Planning (KETEP)
332 and the Ministry of Trade, Industry & Energy (MOTIE) of the Republic of Korea (No. 20201510100020).

333

334 **References**

- 335 [1]. Nakamura, N., Akita, S., Suzuki, T., Koba, M., Nakamura, S., & Nakano, T. (2010). Study of ultimate
336 seismic response and fragility evaluation of nuclear power building using nonlinear three-dimensional
337 finite element model. *Nuclear Engineering and Design*, 240(1), 166-180.
- 338 [2]. Huang, Y. N., Whittaker, A. S., & Luco, N. (2011). A probabilistic seismic risk assessment procedure
339 for nuclear power plants:(I) Methodology. *Nuclear Engineering and Design*, 241(9), 3996-4003.
- 340 [3]. Huang, Y. N., Whittaker, A. S., & Luco, N. (2011). A probabilistic seismic risk assessment procedure
341 for nuclear power plants:(II) Application. *Nuclear Engineering and Design*, 241(9), 3985-3995.
- 342 [4]. Yawson, P. Y., & Lombardi, D. (2018). Probabilistic seismic risk assessment of nuclear reactor in a
343 hypothetical UK site. *Soil Dynamics and Earthquake Engineering*, 113, 278-285.
- 344 [5]. Jussila, V., Li, Y., & Fülöp, L. (2016). Statistical analysis of the variation of floor vibrations in nuclear
345 power plants subject to seismic loads. *Nuclear Engineering and Design*, 309, 84-96.
- 346 [6]. Segarra, J. D., Bensi, M., Weaver, T., & Modarres, M. (2020). Extension of probabilistic seismic hazard
347 analysis to account for the spatial variability of ground motions at a multi-unit nuclear power plant hard-
348 rock site. *Structural Safety*, 85, 101958.
- 349 [7]. Kwag, S., Park, J., & Choi, I. K. (2020). Development of efficient complete-sampling-based seismic
350 PSA method for nuclear power plant. *Reliability Engineering & System Safety*, 197, 106824.
- 351 [8]. Wang, J., & Lin, M. (2018). Seismic probabilistic risk analysis and application in a nuclear power plant.
352 *Nuclear Technology*, 203(3), 221-231.
- 353 [9]. Zhou, T., Modarres, M., & Droguett, E. L. (2018). An improved multi-unit nuclear plant seismic
354 probabilistic risk assessment approach. *Reliability Engineering & System Safety*, 171, 34-47.
- 355 [10]. Banyay, G. A., Shields, M. D., & Brigham, J. C. (2020). Efficient global sensitivity analysis of structural
356 vibration for a nuclear reactor system subject to nonstationary loading. *Nuclear Engineering and Design*,
357 361, 110544.
- 358 [11]. Choi, B., Nishida, A., Li, Y., Muramatsu, K., & Takada, T. (2018). Epistemic Uncertainty Quantification
359 of Floor Responses for a Nuclear Reactor Building. In *International Conference on Nuclear Engineering*
360 (Vol. 51449, p. V002T14A017). American Society of Mechanical Engineers.

- 361 [12]. Choi, B., Nishida, A., Shiomi, T., Muramatsu, K., & Takada, T. (2019). Uncertainty of different
362 modeling methods of NPP building subject to seismic ground motions. Transactions of 25th
363 International Conference on Structural Mechanics in Reactor Technology (SMiRT-25), Charlotte, NC,
364 USA.
- 365 [13]. Lyons, S., & Vasavada, S. (2018). Seismic Probabilistic Risk Assessment of Nuclear Power Plants: 10
366 CFR 50.69 Assumptions and Sources of Uncertainty. In ASME International Mechanical Engineering
367 Congress and Exposition (Vol. 52187, p. V013T05A047). American Society of Mechanical Engineers.
- 368 [14]. Kim, J. H., Choi, I. K., & Park, J. H. (2011). Uncertainty analysis of system fragility for seismic safety
369 evaluation of NPP. *Nuclear Engineering and Design*, 241(7), 2570-2579.
- 370 [15]. Syed, S., & Gupta, A. (2015). Seismic fragility of RC shear walls in nuclear power plant part 2: Influence
371 of uncertainty in material parameters on fragility of concrete shear walls. *Nuclear Engineering and
372 Design*, 295, 587-596.
- 373 [16]. Chen, W., Zhang, Y., & Wang, D. (2021). Damage development analysis of the whole nuclear power
374 plant of AP1000 type under strong main-aftershock sequences. *Nuclear Engineering and Design*, 371,
375 110975.
- 376 [17]. Bao, X., Zhang, M. H., & Zhai, C. H. (2019). Fragility analysis of a containment structure under far-
377 fault and near-fault seismic sequences considering post-mainshock damage states. *Engineering
378 Structures*, 198, 109511.
- 379 [18]. Choi, I. K., Choun, Y. S., Ahn, S. M., & Seo, J. M. (2008). Probabilistic seismic risk analysis of CANDU
380 containment structure for near-fault earthquakes. *Nuclear Engineering and Design*, 238(6), 1382-1391.
- 381 [19]. Nguyen, D. D., Thusa, B., & Lee, T. H. (2018). Seismic fragility of base-isolated nuclear power plant
382 considering near-fault ground motions. *Journal of the Korean Society of Hazard Mitigation*, 18(7), 315-
383 321.
- 384 [20]. Jin, S., & Gong, J. (2020). Damage performance based seismic capacity and fragility analysis of existing
385 concrete containment structure subjected to near fault ground motions. *Nuclear Engineering and
386 Design*, 360, 110478.

- 387 [21]. Jin, S., Rong, H., & Lyu, X. (2021). Probabilistic seismic performance evaluation of nuclear
388 containment structure subjected to far-fault ground motions. *Structures*, 32, 2232-2246.
- 389 [22]. Zhao, C., Yu, N., Oz, Y., Wang, J., & Mo, Y. L. (2020). Seismic fragility analysis of nuclear power
390 plant structure under far-field ground motions. *Engineering Structures*, 219, 110890.
- 391 [23]. Cho, S. G., & Joe, Y. H. (2005). Seismic fragility analyses of nuclear power plant structures based on
392 the recorded earthquake data in Korea. *Nuclear engineering and design*, 235(17-19), 1867-1874.
- 393 [24]. Medel-Vera, C., & Ji, T. (2016). Seismic probabilistic risk analysis based on stochastic simulation of
394 accelerograms for nuclear power plants in the UK. *Progress in Nuclear Energy*, 91, 373-388.
- 395 [25]. Nguyen, D. D., Thusa, B., & Lee, T. H. (2019). Effects of Significant Duration of Ground Motions on
396 Seismic Responses of Base-Isolated Nuclear Power Plants. *Journal of the Earthquake Engineering
397 Society of Korea*, 23(3), 149-157.
- 398 [26]. Van Nguyen, D., Kim, D., & Nguyen, D. D. (2020). Nonlinear seismic soil-structure interaction analysis
399 of nuclear reactor building considering the effect of earthquake frequency content. In *Structures*, 26,
400 901-914.
- 401 [27]. Nguyen, D. D., Thusa, B., Han, T. S., & Lee, T. H. (2020). Identifying significant earthquake intensity
402 measures for evaluating seismic damage and fragility of nuclear power plant structures. *Nuclear
403 Engineering and Technology*, 52(1), 192-205.
- 404 [28]. Nguyen, D. D., Thusa, B., Park, H., Azad, M. S., & Lee, T. H. (2021). Efficiency of various structural
405 modeling schemes on evaluating seismic performance and fragility of APR1400 containment
406 building. *Nuclear Engineering and Technology*, 53(8), 2696-2707.
- 407 [29]. Lee SC, Kipkorir KB, Choi Y, Kim HB, Oh CH, Thanh NB (2016). Effective Prestress Force
408 Considering Instantaneous Loss in Reactor Containment Building.” *International Journal of
409 Engineering Research and Development*, 12(11), 18-23.
- 410 [30]. Basha, S. M., Singh, R. K., Patnaik, R., Ramanujam, S., Kushwaha, H. S., & Raj, V. V. (2003).
411 Predictions of ultimate load capacity for pre-stressed concrete containment vessel model with BARC
412 finite element code ULCA. *Annals of Nuclear Energy*, 30(4), 437-471.

- 413 [31]. Hu, H. T., & Lin, Y. H. (2006). Ultimate analysis of PWR prestressed concrete containment subjected
414 to internal pressure. *International journal of pressure vessels and piping*, 83(3), 161-167.
- 415 [32]. Chakraborty, M. K., Acharya, S., Pisharady, A. S., Roshan, A. D., & Bishnoi, L. R. (2017). Assessment
416 of Ultimate Load Capacity of concrete containment structures against structural collapse. *Nuclear*
417 *Engineering and Design*, 323, 417-426.
- 418 [33]. Tavakkoli, I., Kianoush, M. R., Abrishami, H., & Han, X. (2017). Finite element modelling of a nuclear
419 containment structure subjected to high internal pressure. *International Journal of Pressure Vessels and*
420 *Piping*, 153, 59-69.
- 421 [34]. Yan, J., Lin, Y., Wang, Z., Fang, T., & Ma, J. (2019). Failure mechanism of a prestressed concrete
422 containment vessel in nuclear power plant subjected to accident internal pressure. *Annals of Nuclear*
423 *Energy*, 133, 610-622.
- 424 [35]. Rizkalla, S. H., Simmonds, S. H., & MacGregor, J. G. (1984). Prestressed concrete containment
425 model. *Journal of Structural Engineering*, 110(4), 730-743.
- 426 [36]. Twidale, D., & Crowder, R. (1991). Sizewell 'B'-A one tenth scale containment model test for the UK
427 PWR programme. *Nuclear engineering and design*, 125(1), 85-93.
- 428 [37]. Hessheimer, M. F., Shibata, S., & Costello, J. F. (2003). Functional and Structural Failure Mode
429 Overpressurization Tests of 1: 4-Scale Prestressed Concrete Containment Vessel Model (H372).
- 430 [38]. Kevorkian, S., Heinfling, G., & Courtois, A. (2005). Prediction of a containment vessel mock-up
431 cracking during over design pressure test.
- 432 [39]. Sandia National Laboratories, 2000. Pretest Round Robin Analysis of a Prestressed Concrete
433 Containment Vessel Model. U.S. Nuclear Regulatory Commission (NRC) and Nuclear Power
434 Engineering Corporation (NUPEC), NUREG/CR-6678.
- 435 [40]. Yonezawa, K., Imoto, K., Watanabe, Y., & Akimoto, M. (2002). Ultimate capacity analysis of 1/4
436 PCCV model subjected to internal pressure. *Nuclear engineering and design*, 212(1-3), 357-379.
- 437 [41]. Choun, Young-Sun, and Junhee Park (2015). Evaluation of seismic shear capacity of prestressed
438 concrete containment vessels with fiber reinforcement. *Nuclear Engineering and Technology* 47(6),
439 756-765.

- 440 [42]. Choun, Y. S., & Park, H. K. (2015). Containment performance evaluation of prestressed concrete
441 containment vessels with fiber reinforcement. *Nuclear Engineering and Technology*, 47(7), 884-894.
- 442 [43]. ANSYS, Inc. (2019). ANSYS mechanical APDL element reference.
- 443 [44]. Lee S. C, Kipkorir K. B., Choi Y., Kim H. B., Oh C. H., and Nhu B. T. (2016). Effective prestress force
444 considering instantaneous loss in reactor containment building. *International Journal of Engineering
445 Research and Development*, 12(11).
- 446 [45]. Li, C., Zhai, C., Kunnath, S., & Ji, D. (2019). Methodology for selection of the most damaging ground
447 motions for nuclear power plant structures. *Soil Dynamics and Earthquake Engineering*, 116, 345-357.
- 448 [46]. Cho, H., Koh, H. M., Hyun, C. H., & Shin, H. M. (2004). Seismic damage assessment of nuclear power
449 plant containment structures. In *13th World Conference on Earthquake Engineering*, Vancouver,
450 Canada.

Declaration of interests

The authors declare that they have no known competing financial interests or personal relationships that could have appeared to influence the work reported in this paper.

Journal Pre-proof